

This work was written as part of one of the author's official duties as an Employee of the United States Government and is therefore a work of the United States Government. In accordance with 17 U.S.C. 105, no copyright protection is available for such works under U.S. Law.

Public Domain Mark 1.0






<https://creativecommons.org/publicdomain/mark/1.0/>

Access to this work was provided by the University of Maryland, Baltimore County (UMBC) ScholarWorks@UMBC digital repository on the Maryland Shared Open Access (MD-SOAR) platform.

Please provide feedback

Please support the ScholarWorks@UMBC repository by emailing scholarworks-group@umbc.edu and telling us what having access to this work means to you and why it's important to you. Thank you.

Extended Line Spread Function of TES Microcalorimeters With Au/Bi Absorbers

Megan E. Eckart , Joseph S. Adams, Simon R. Bandler, Sophie Beaumont, James A. Chervenak, Aaron M. Datesman , Fred M. Finkbeiner , Ruslan Hummatov, Richard L. Kelley, Caroline A. Kilbourne , Maurice A. Leutenegger, Antoine R. Miniussi, Samuel J. Moseley, F. Scott Porter, John E. Sadleir, Kazuhiro Sakai, Stephen J. Smith, Nicholas A. Wakeham , and Edward J. Wassell

Abstract—Microcalorimeters have the potential to provide line shapes well described by a single Gaussian broadening term of few-eV width. This attribute makes the detectors especially well suited for x-ray astrophysics observations; however, low-level non-Gaussian broadening terms are expected and must be characterized. These terms depend on the composition of the x-ray absorber, the detailed x-ray absorption physics, the device thermalization processes, and the incident x-ray energy. Here we present the first measurements targeted at understanding the extended line-spread function (LSF) of x-ray microcalorimeter pixels under development for the X-ray Integral Field Unit on the Athena X-ray Observatory. These pixels are composed of Mo/Au transition-edge sensors with overhanging electroplated Au/Bi absorbers. We have measured the line shapes using monochromatic x-ray sources with <1-eV width at several x-ray energies (0.85, 0.93, 1.25, 1.5, 5.4, and 8.0 keV) across the instrument bandpass (0.3–12 keV) and have modeled the line profiles. These results are compared to the extended LSF of the *Hitomi* microcalorimeter pixels that used HgTe absorbers.

Index Terms—x-ray detectors, Superconducting devices, Astrophysics.

I. INTRODUCTION

ARRAYS of microcalorimeter detectors built at NASA's Goddard Space Flight Center (GSFC) will be used to provide high resolution imaging spectroscopy for the Athena X-ray

Observatory's X-ray Integral Field Unit (X-IFU) [1]. These devices use transition-edge sensors (TESs) with Mo/Au bilayers and overhanging Au/Bi absorbers to provide ≈ 2 eV full-width at half-maximum (FWHM) energy resolution. Measurements to characterize the spectral performance of prototype detectors often rely on photons from ^{55}Fe sources or fluorescent targets and focus on measuring the Gaussian broadening that dominates the instrument line spread function; however, energy loss mechanisms in the absorber can lead to additional features. We call these additional features the extended line spread function.

We studied and calibrated these features for the *Hitomi* (Astro-H) Soft x-ray Spectrometer (SXS) detectors that used silicon thermistor microcalorimeters with HgTe absorbers [2]. We found that a small fraction of events are redistributed to lower energies due to several energy loss mechanisms in the absorber, resulting in 1) a low-energy exponential tail, 2) the so-called electron-loss continuum, which was empirically found to have roughly constant flux per unit energy interval, 3) escape peaks due to x-ray fluorescence photons that may escape from the absorber instead of being thermalized, and 4) a small Si K fluorescence peak.

In this work, we aim to understand the nature and origin of the extended line spread function for our TES detectors with electroplated Au/Bi absorbers, slated for upcoming ground and space instruments. Understanding this is important for a few reasons: for x-ray spectroscopy applications we must know our instrument response to correctly interpret measured line shapes, and for detector development we must understand the device absorption physics. Practically, we must ensure that measurements of device performance are not confused by the convolution of extended LSF features with the complicated natural line complexes often used for device characterization.

Our approach for this initial study is to illuminate TES pixels with Au/Bi absorbers suitable for the Athena X-IFU with monochromatic x-rays. We will measure the low-energy exponential tail (or upper limit) at each energy with a goal of determining where in the absorber energy loss occurs. For example, does the feature arise from events absorbed near the absorber surface or in a particular layer of the absorber? We are undertaking this study now to provide a first estimate of the full energy redistribution function for Athena mission planning. We also aim to aid in understanding why we occasionally have

Manuscript received October 31, 2018; accepted March 1, 2019. Date of publication March 6, 2019; date of current version June 6, 2019. This work was performed in part under the auspices of the U.S. Department of Energy, by Lawrence Livermore National Laboratory under Contract DE-AC52-07NA27344. (Corresponding author: Megan E. Eckart.)

M. E. Eckart was with NASA Goddard Space Flight Center, Greenbelt, MD 20771 USA. She is now with Lawrence Livermore National Laboratory, Livermore, CA 94550 USA (e-mail: eckart2@llnl.gov).

J. S. Adams, S. Beaumont, R. Hummatov, M. A. Leutenegger, A. R. Miniussi, K. Sakai, S. J. Smith, and N. Wakeham are with NASA Goddard Space Flight Center, Greenbelt, MD 20771 USA, and also with CRESST, University of Maryland–Baltimore County, Baltimore, MD 20742 USA.

S. R. Bandler, J. A. Chervenak, R. L. Kelley, C. A. Kilbourne, F. S. Porter, and J. E. Sadleir are with NASA Goddard Space Flight Center, Greenbelt, MD 20771 USA.

A. M. Datesman, S. J. Moseley, and E. J. Wassell are with NASA Goddard Space Flight Center, Greenbelt, MD 20771 USA, and also with Stinger-Ghaffarian Technologies, Inc., Greenbelt, MD 20771 USA.

F. M. Finkbeiner is with NASA Goddard Space Flight Center, Greenbelt, MD 20771 USA, and also with Sigma Space, Lanham, MD 20706 USA.

Color versions of one or more of the figures in this paper are available online at <http://ieeexplore.ieee.org>.

Digital Object Identifier 10.1109/TASC.2019.2903420

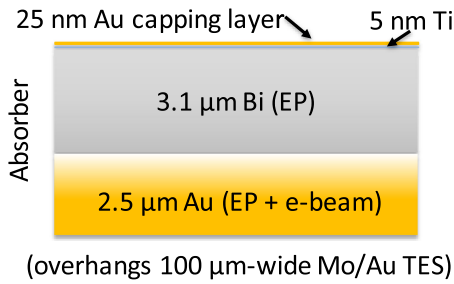


Fig. 1. Cartoon illustrating the absorber layer composition. The thick bottom Au provides good device thermalization and the Bi layer increases the x-ray stopping power with minimal additional heat capacity. These thick layers are electroplated on a 200 nm-thick Au e-beam evaporated seed layer. The top Au capping layer was added to increase the device reflectance in the optical and infrared. The thin Ti is used as a sticking layer. Not shown is an additional 10 nm Ti sticking layer at the bottom of the absorber stack.

outlier wafers, chips, or pixels with degraded resolution or a large fraction of events in a low-energy tail.

II. EXPERIMENTAL SETUP

A. Microcalorimeter Design

For this experiment we aimed to study a device that is a prototype pixel for the X-IFU. Standard performance testing was completed before our experiment. We chose a device that has a reasonable measured heat capacity and exhibits no significant spectral degradation compared to that predicted based on measurements of the signal and noise. The device has a transition temperature, T_c , of 107 mK, higher than the X-IFU target of 90 mK, but acceptable for these tests. The TESs are $100\ \mu\text{m} \times 100\ \mu\text{m}$ Mo/Au squares of thickness 35 nm/108 nm on a $0.5\ \mu\text{m}$ -thick SiN membrane. Au banks of 190 nm thickness and $6\ \mu\text{m}$ width have $3\ \mu\text{m}$ overlap with the sides of the TES parallel to the direction of current flow, and the Nb electrical leads contact the TES at the opposite edges. These devices do not have the added Au features perpendicular to the direction of current flow ('stripes') that had been routinely used for noise mitigation but could cause undesirable features in the superconducting transition [3]. The device normal resistance, R_n , is $\sim 28\ \text{m}\Omega$. The thick electroplated absorbers are described in Figures 1 and 2. Two round stems with $10\ \mu\text{m}$ diameter connect the absorber to the TES banks, and four additional stems of $4\ \mu\text{m}$ diameter add mechanical support but do not electrically contact the TES. A $2\ \mu\text{m}$ -thick Cu layer was deposited onto the back of the silicon wafer and $\sim 60\%$ up the sidewalls of the silicon wells beneath each pixel to increase the array heat sinking.

B. X-ray Monochromators

We measured the detector line spread function using several monochromators. This equipment was used for *Hitomi* SXS ground calibration and is described in Ref. [2]; we provide brief summaries here. At low energies ($< 2\ \text{keV}$) we used a surface normal rotation (SNR) grating monochromator to provide monochromatic lines of width $\sim 1\ \text{eV}$ FWHM. Please see Figure 3 for more details. At higher energies we used portable

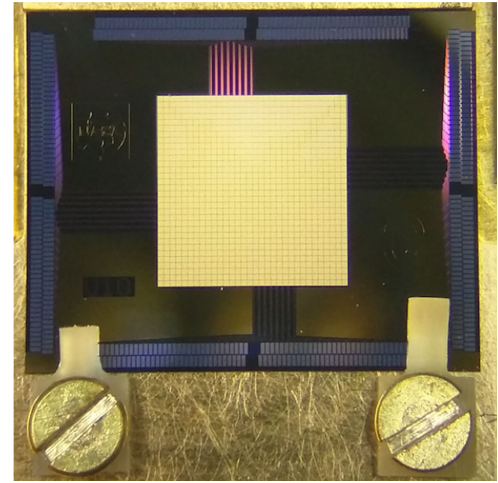


Fig. 2. Optical microscope photo of the GSFC-built kilopixel array under test. The chip size is $15\ \text{mm} \times 19\ \text{mm}$. The array pitch is $250\ \mu\text{m}$ and each absorber is $240\ \mu\text{m} \times 240\ \mu\text{m}$.

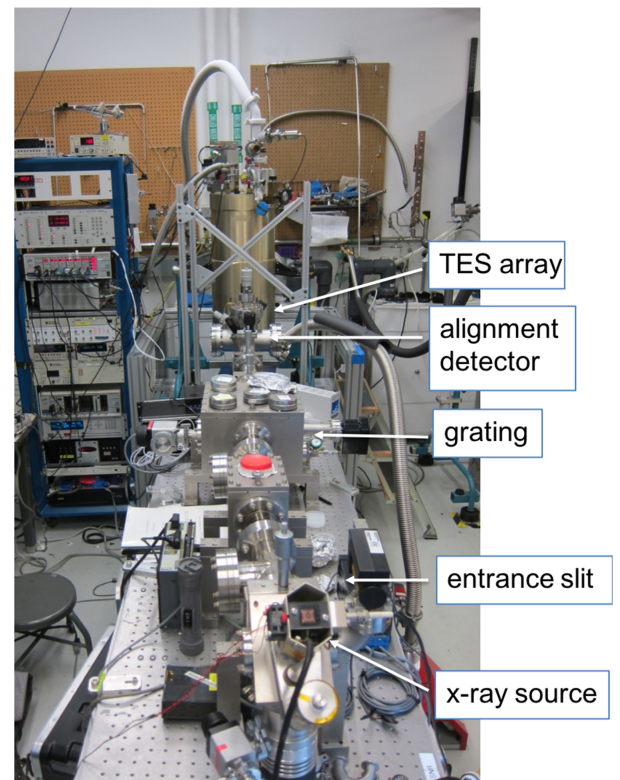


Fig. 3. Surface normal rotating (SNR) monochromator [4] attached to our laboratory TES characterization platform. x-rays pass through an entrance slit and a collimating optic for the cross-dispersion direction, are diffracted from a reflection grating, which focuses the incident diverging beam at the exit slit, and then made monochromatic by the exit slit. The x-ray source [5] has changeable anodes and for each exposure we rotate the grating to match the $K\alpha_1$ or $L\alpha_1$ emission from the source anode. For this experiment we used Ni, Cu, Mg, and Al anodes to provide $0.2 - 1.5\ \text{ct s}^{-1}\ \text{pixel}^{-1}$.

channel-cut crystal monochromators (CCCMs) built at GSFC [6]. A commercial x-ray tube illuminates a pair of channel-cut crystals that are aligned in a dispersive configuration to select the $K\alpha_1$ line of the anode material. In this experiment we used Si (220) channel-cut crystals with a Cr-anode Oxford x-ray tube

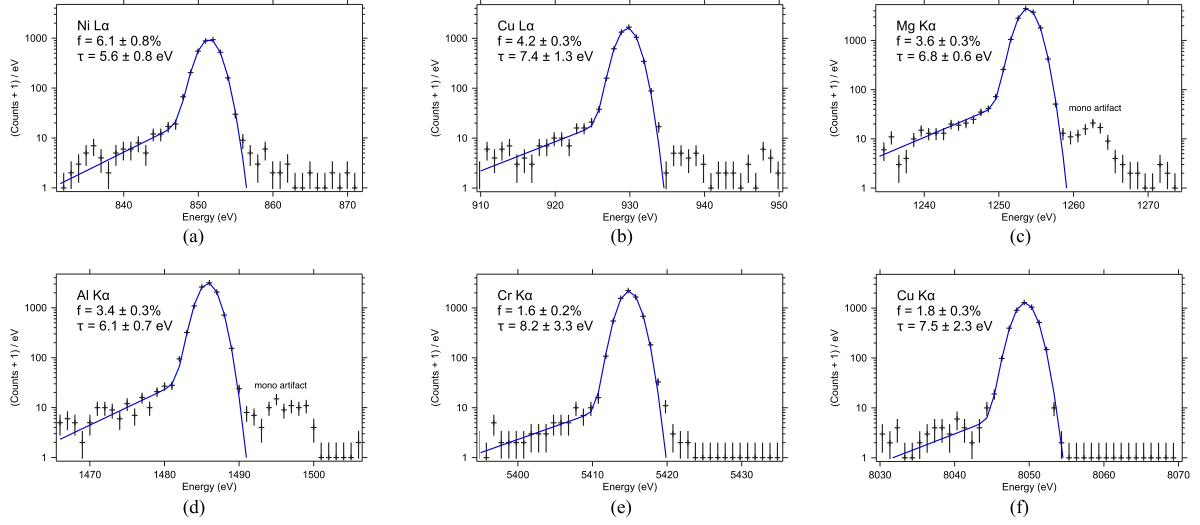


Fig. 4. Measured spectra (black crosses) with 1 eV binning. Fits to each histogram are overlaid in blue. We perform a non-linear least-squares fit with weights equal to the square root of the data; however, we add 1 to each bin to remove zero count bins before fitting, as illustrated in these plots. This method [7] has been shown to work well for fitting spectra containing bins with low counts, similar to the maximum likelihood method presented in Ref. [8]. The labels in each panel indicate the characteristic x-ray line used as input to the monochromator and the best-fit loss fraction (f) and energy decay scale (τ).

and Si (400) crystals with a Cu-anode Oxford x-ray tube to provide lines at 5.4 and 8.0 keV with energy widths of < 0.5 eV FWHM. We have additional CCCMs that provide the line energies shown in Figure 6 b, but these were not used in this preliminary study.

III. X-RAY MEASUREMENTS

We measured a single TES device from the array described in Section II-A. It was cooled in our laboratory adiabatic demagnetization refrigerator (ADR) to a heatsink temperature of 55 mK. We biased the device at 10% R/R_n using a shunt resistor of 0.182 m Ω . We used three aluminized polyimide optical blocking filters within the dewar, for a total filter thickness of 300 nm of aluminum and 3 μ m polyimide. These relatively thick filters prohibited measurements at the lowest x-ray energies (see shaded region in Figure 6 a).

The results of the measurements are presented in Figure 4. Each panel shows a measurement using a different monochromatic line energy. The histograms are fit using a Gaussian broadening term plus an exponential energy loss function convolved with a normalized Gaussian:

$$LSF(E) = (1 - f) G(E - E_o; \sigma) + f F_{\text{exp}}(E - E_o; \sigma, \tau), \quad (1)$$

where E_o is the incident photon energy, E is the redistributed energy (i.e., measured energy), G is a normalized Gaussian, F_{exp} is the exponential energy loss function convolved with a normalized Gaussian (see below), σ is the width of the Gaussian, f is the fraction of events that experience energy loss, and τ is the energy loss decay scale. $F_{\text{exp}}(E - E_o; \sigma, \tau)$ can be analytically evaluated to:

$$\frac{1}{2\tau} e^{\frac{\sigma^2}{2\tau^2}} e^{\frac{(E-E_o)}{\tau}} \left[1 - \text{erf}\left(\frac{E - E_o + \frac{\sigma^2}{\tau}}{\sigma\sqrt{2}}\right) \right]. \quad (2)$$

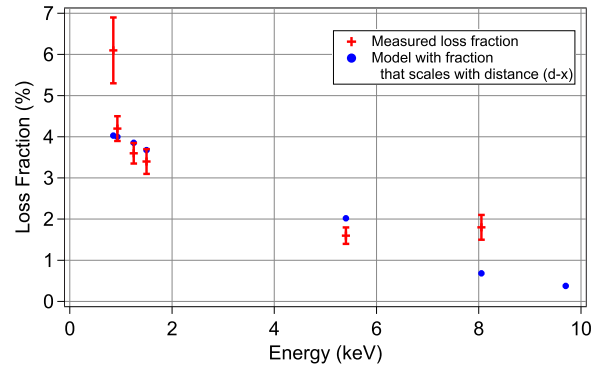


Fig. 5. Measured loss fraction vs incident x-ray energy, using the best-fit values presented in Figure 4. The model values are described in Section IV.

The best-fit parameters for the exponential tail are labeled on the graph. In the case of the SNR monochromator, particularly at Mg K α and Al K α , there are known monochromator artifacts just above the primary line. The number of counts in each spectrum was limited by the x-ray source count rate at the detector pixel (≈ 0.2 –2 cts s $^{-1}$), the laboratory test dewar hold time, and schedule constraints.

IV. DISCUSSION

We find that the fraction of events in the low-energy tail depends on energy. Figure 5 summarizes the loss fraction measurements. We find that the decay scale of the energy loss, τ , is approximately 6 eV and does not vary significantly with incident x-ray energy. Overall, these results are promising for the Athena X-IFU. While the low-energy tail will need to be calibrated across the instrument bandpass, the performance will not be significantly degraded since the loss fraction is low.

A recent study using 4.5–8.0 keV fluorescent x-rays found that pixels with evaporated Bi absorbers showed a very large

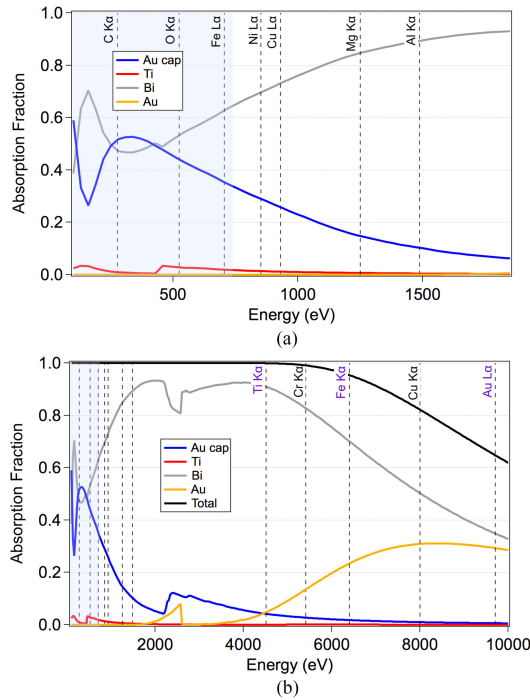


Fig. 6. (a) Event absorption fraction in each absorber layer as a function of incident x-ray energy. We use literature values of the density and mass absorption coefficients [10]. The total absorption is unity across this energy range. The vertical dashed lines indicate the lines generated by the SNR monochromator. The shaded region indicates a region where the low transmission of the relatively thick optical blocking filters in the dewar prohibits characterization measurements. (b) Same curves as in (a), but the range is expanded to 10 keV and a curve showing the total transmission is added. The vertical dashed lines from 4.5–9.7 keV indicate lines generated by our channel-cut crystal monochromators (CCCMs). For this experiment we did not make measurements at the lines labeled in purple (Ti K α , Fe K α , and Au L α) due to schedule constraints.

(>20%) low-energy exponential tail that was much reduced in comparable devices with electroplated Au/Bi or Au-only absorbers [9]. Our results are consistent with the notion that devices with electroplated absorbers typically exhibit relatively low loss fractions.

To investigate the origin of the low-energy tail, we compare the trend in Figure 5 to the curves in Figure 6, which illustrate the fraction of events absorbed in each layer of the absorber. We find that the measured loss fraction does not correlate with event probabilities of absorption in a particular layer of the absorber. This result holds if we consider the $\sim 0.5 \mu\text{m}$ RMS average surface roughness of the Bi. Similarly, if we compute the fraction of events absorbed near the Au surface or near the Bi surface, we cannot explain the measured loss fractions. The measured points at 5.4 and 8.0 keV are particularly hard to fit with a model related to surface absorption, which falls off much more quickly with increasing x-ray energy than the measurements. In contrast, for the *Hitomi* SXS the fraction of events in the tail varied with x-ray energy in a manner consistent with the fraction of events absorbed near the surface of the HgTe [2].

We investigated models with loss probabilities that scale with the distance from the absorption location to the thick Au layer, postulating that the energy loss or trapping occurs in the Bi during the energy downconversion process following x-ray

absorption. In our toy model, absorption events in the Bi were scaled by $(d - x)$, where d is the Bi thickness and x is the absorption location with $x = 0$ at the top of the Bi; events absorbed in the capping layer were scaled by d ; and events absorbed in the bottom Au layer were assumed to experience no energy loss. Integrating this scaling function over the probability of absorption at each location produced a curve that was closest to the measured values: a curve that decays more slowly with increasing energy (see Figure 5). Still, this model predicts that the loss fraction at Cu K α will be < 1% and smaller than that of Cr K α , which does not match the data. None of the mechanisms we considered gave any indication for why the Ni L α line at 0.85 keV would have a much larger tail than the neighboring measurement at Cu L α at 0.93 keV.

The fraction of events that experience energy loss is higher than those measured for the *Hitomi* SXS devices with HgTe absorbers. From 0.85–1.5 keV the loss fractions are ~ 3 times higher; however, the difference is more striking at higher energies. At 5.4 and 8.0 keV we measured significant detections of $\sim 2\%$ loss fraction in this device, but upper limits of 0.1% for SXS.

We have so far concentrated on finding a single mechanism to explain the measured results but it is possible that more than one mechanism is required. This could take the form of two separate absorption depth dependent effects or involve lateral position dependent effects as well. Additional data – at a wider range of line energies and with higher statistics – is essential.

V. CONCLUSION AND FUTURE WORK

We have studied the extended line spread function of TES microcalorimeters with Au/Bi absorbers targeted for the Athena X-IFU. We measured the response to monochromatic x-rays from 0.85–8.0 keV, and found a low-level, low-energy exponential tail at all energies that we ascribe to energy loss in the absorber. The fraction of events in the tail varies from 1.6 to 6.1%, with an energy decay scale of ~ 6 eV that is independent of incident energy. Overall, the low fraction of events in the tail is promising for upcoming instruments: while we will need to calibrate this effect, it should not significantly affect the instrument performance. We are studying the energy scaling of the loss fraction to understand the origin of the events that contribute to the tail. The results to-date do not correlate with the absorption fraction of events in a particular layer in the absorber or near a surface, unlike the case of our previous study of the *Hitomi* microcalorimeters that used HgTe absorbers. It may be that there is more than one mechanism causing the low-energy tail.

This study represents the first measurements of devices with Au/Bi absorbers using monochromatic sources over this range of x-ray energies, and the results are preliminary. Our future work will focus on increasing the counting statistics per line, measuring at the additional x-ray energies shown in Figure 6, measuring a larger suite of pixels, as well as measuring devices from different wafers, which will include devices with Au/Bi absorbers that do not have an Au capping layer.

REFERENCES

- [1] D. Barret *et al.*, “The ATHENA X-ray Integral Field Unit (X-IFU),” *Society of Photo-Optical Instrumentation Engineers (SPIE) Conference Series*, vol. 10699, p. 106991G, Jul. 2018.
- [2] M. E. Eckart *et al.*, “Ground calibration of the Astro-H (Hitomi) soft x-ray spectrometer,” *J. Astron. Telesc. Instrum. Syst.*, vol. 4, no. 2, p. 021406, Apr. 2018.
- [3] N. A. Wakeham *et al.*, “Effects of normal metal features on superconducting transition-edge sensors,” *J. Low Temp. Phys.*, vol. 193, no. 3-4, pp. 231–240, Nov. 2018.
- [4] M. C. Hettrick, “Surface normal rotation: A new technique for grazing-incidence monochromators,” *Appl. Opt.*, vol. 31, pp. 7174–7177, Dec. 1992.
- [5] “Manson Model 2 Mini-Focus Ultrasoft x-ray Source,” [Online]. Available: <http://www.austinst.com/model2.html>. Accessed: Feb. 26, 2019.
- [6] M. A. Leutenegger *et al.*, “Compact, low-cost, high-resolution monochromatic x-ray source for characterization of x-ray calorimeter arrays,” submitted for publication.
- [7] K. J. Mighell, “Parameter estimation in astronomy with Poisson-distributed data. I. The χ^2_γ statistic,” *Astrophysical J.*, vol. 518, pp. 380–393, Jun. 1999.
- [8] J. W. Fowler, “Maximum-likelihood fits to histograms for improved parameter estimation,” *J. Low Temp. Phys.*, vol. 176, no. 3, pp. 414–420, Aug. 2014.
- [9] D. Yan *et al.*, “Eliminating the non-Gaussian spectral response of x-ray absorbers for transition-edge sensors,” *Appl. Phys. Lett.*, vol. 111, no. 19, p. 192602, Nov. 2017.
- [10] B. L. Henke, E. M. Gullikson, and J. C. Davis, “X-ray interactions: Photoabsorption, scattering, transmission, and reflection at $E = 50\text{--}30,000$ eV, $Z = 1\text{--}92$,” *Atomic Data Nucl. Data Tables*, vol. 54, pp. 181–342, Jul. 1993.